Self-assembled chitosan polymer intercalating peptide functionalized gold nanoparticles as nanoprobe for efficient imaging of urokinase plasminogen activator receptor in cancer diagnostics

Deepshikha Shahdeo [a], Veerbhan Kesarwani [a], Deepa Suhag [b], Jahangeer Ahmed [c], Saad M. Alshehri [c], Sonu Gandhi [a,d,*]

[a] DBT-National Institute of Animal Biotechnology (DBT-NIAB), Hyderabad 500032, Telangana, India
[b] Amity Institute of Biotechnology, Amity University Haryana, Manesar, Panchgaon, Haryana 122413, India
[c] Department of Chemistry, College of Science, King Saud University, Riyadh 11451, Saudi Arabia
[d] Amity Institute of Biotechnology, Amity University, Noida 201301, India

A B S T R A C T

Targeting cell surface receptors for specific drug delivery in cancer has garnered lot of attention. Urokinase plasminogen activator receptor (uPAR), a surface biomarker, is overexpressed on many tumours including breast, colorectal, prostate, and ovarian cancers. Binding of growth factor domain (GFD) of urokinase plasminogen activator (uPA) with uPAR lead to its close conformation, and allow somatomedin B domain (SMB) of vitronectin binding by allosteric modulation. In-silico docking of uPAR with GFD and SMB peptides was performed to identify potential binding affinity. Herein, we report fluorescently labeled peptide functionalized AuNPs with a mixed self-assembled monolayer of intercalating chitosan polymer for efficient targeting and imaging of uPAR-positive cells. The biophysical characterization of nanoconjugates and uPAR-specific targeting was assessed by FACS, cell adhesion, and fluorescence imaging. AuNPs/chitosan/GFD+SMB peptides showed higher uptake as compared to AuNPs/chitosan/GFD, and AuNPs/chitosan/SMB that can be utilized as a tool for molecular targeting and imaging in metastasis.

1. Introduction

Urokinase plasminogen activator receptor (uPAR) is a glycosylphosphatidylinositol (GPI) anchored receptor that plays a significant role in extracellular matrix invasion, cell adhesion, migration, and metastasis (Andreasen, Egelund, & Petersen, 2000; Avvakumova et al., 2014; Bachran & Leppla, 2016). uPAR is overexpressed on various cancer cells, including oral, breast, lung, ovary, and head and neck cancer (Clogston & Patri, 2011; Duffy, 2004; Fedorova et al., 2011). Urokinase plasminogen activator (uPA) and vitronectin (Vn) bind at different sites in uPAR for the coordinated regulation of cell adhesion and migration (Kalimuthu et al., 2018). High affinity (uPA-uPAR interaction) is mediated by binding with its amino terminal growth factor domain (ATF or GFD; growth factor domain) while moderate affinity (Vn-uPAR interaction) is achieved by binding with its N terminal somatomedin B (SMB) domain (Khanna et al., 2011; Kjaergaard, Hansen, Jacobsen, Gardsvoll, & Ploug, 2008).

Binding of uPA and uPAR led to closed active conformation that drives affinity of Vn to uPAR and activates intracellular signaling and plasminogen activation (MacDonald, DeClerck, & Laug, 1998; Madsen, Ferraris, Andolfo, Cunningham, & Sidenius, 2007; Magnussen et al., 2017). Unbound uPAR usually exists in an open conformation having less affinity for SMB (Kjaergaard et al., 2008). Growing body of evidence suggests that uPA-uPAR interaction allows Vn binding by allosteric modulation (of the SMB binding site) on the cell surface in uPAR dependent manner (Zhao et al., 2015a, 2015b). Importantly, these recently discovered allosteric effects of GFD and SMB provide a promising novel drug target for the treatment of cancer.

Overexpression of protease is an effective tool for the detection of biomarkers of cancer such as urokinase plasminogen activator receptor (uPAR) (Gandhi, Arami, & Krishnan, 2016; Molino et al., 2017; Roberts, Tripathi, & Gandhi, 2019). Various strategies have been developed for uPAR targeting and imaging, which include uPA-activated prodrugs, (Carriero et al., 1997; Mauro et al., 2017) targeted radiotherapy,

(Munhoz et al., 2014) monoclonal antibodies (mAbs), (Avvakumova et al., 2014; Clogston & Patri, 2011) and small molecule/peptide inhibitors (Lee, 2015; Nykjar, 1997; Pavón et al., 2016). Radioisotopes have also been used for the detection of protease which offers highly sensitive and precise assays but also has several drawbacks such as short half-life, personal safety, and environmental concern.

However, peptide-based targeting has shown to be the most successful and convenient method (Ploug et al., 2001; Rakashanda, Rana, Rafiq, Masood, & Amin, 2012). In the past few decades, numerous peptide-based ligands have been described, such as ATF/GFD peptide sequence derived from uPA for uPAR targeting, (Rea et al., 2013; Roberts et al., 2019) $\alpha_9\beta_1$ integrin receptor-targeting peptides, (Chikkaveeraiah, Bhirde, Morgan, Eden, & Chen, 2012; Medley et al., 2008; Ploug et al., 2001) and ApoE peptides for LDL receptor (Tamir et al., 2016). This upsurge in the adoption of peptide-based, receptor-mediated targeting for cancer diagnostics is ascribed to its ability to exclude undesirable natural biological activities, regular and density-controlled distribution of ligands, and escape of nonspecific uptake by reticuloendothelial system (Caracciolo et al., 2013). In addition, peptide-based ligands are chemically stable, less immunogenic, avoid outgrowth of drug-resistant cells and in contrast to mAbs, can be easily tailored (Tripathi, Arami, Banga, Gupta, & Gandhi, 2018; Wang, Löwik, Miller, & Thanou, 2009). Notwithstanding the fact that peptide-based ligands confer myriad benefits, they also have to endure several handicaps such as instability, and enzymatic hydrolysis in liver, kidney, and blood (Wang et al., 2009). These hurdles of peptide-based targeting could be overcome by conjugation of the peptides with nanoparticles, which can improve the pharmacokinetic and pharmacodynamic properties of the peptide.

Gold nanoparticles (AuNPs) act as potential probes for the attachment of peptides as they have unique physiochemical, and optical properties which make them highly compatible for conjugation with small biomolecules like DNA, proteins, enzymes, and amino acids (Tian, Yang, Wang, & Yuan, 2014). Avvakumova et al. have developed a biocompatible, fluorescent labeled AuNPs functionalized U11 peptide for targeting of uPAR in cancer (Avvakumova et al., 2014). Use of polymers, such as chitosan due to its positive charge, biodegradability, less toxicity, mucoadhesive properties, and pH responsiveness, had been widely used as an effective carrier in delivery of proteins, drugs, DNA, and peptides (Ansari et al., 2016; Chew, Wolfowicz, Mao, Leong, & Chua, 2003; Mohammed, Syeda, Wasan, & Wasan, 2017). Coating of chitosan with AuNPs improves its bioavailability as it had been utilized for probing, imaging in case of tumour targeting (Chen, Wang, Chen, Xu, & Liu, 2013; Duan et al., 2014).

Herein, we compared the binding affinity of GFD and SMB peptides with uPAR separately and in a close proximity. Therefore, the present study reports the development of AuNPs functionalized peptide (GFD and SMB) mediated efficient targeting of uPAR-overexpressing cells (Hettiarachchi, Prasai, & McCarley, 2014; Wang et al., 2014). Further, this study tests the hypothesis whether AuNPs functionalized with SMB peptide shows improved targeting and robust imaging when present cooperatively with GFD peptide in a similar manner as for the GFD and SMB ligands (Hettiarachchi et al., 2014; Sidenius, Andolfo, Fesce, & Blasi, 2002; Waltz & Chapman, 1994; Zhao et al., 2015a, 2015b). In support of this hypothesis, we have conducted numerous experiments such as uptake assay, cell adhesion assay, fluorescence imaging, and FACS. The design and development of GFD and SMB peptides and its characterization was done by High performance liquid chromatography (HPLC), and Matrix-Assisted Laser Desorption/Ionization-Time Of Flight (MALDI-TOF). Synthesis of AuNPs, coating with polymer, and its functionalization with peptides (GFD and SMB) were done in a sequential manner for targeting and imaging of uPAR. For this, AuNPs stabilized with polymer (chitosan) were synthesized and covalently conjugated with uPAR-specific linker peptide sequences with fluorescein isothiocyanate (FITC) at —N terminal of GFD and SMB. The free amine group of AuNPs/chitosan (NH_2-) were coupled with carboxyl group of uPAR-

specific GFD and SMB peptides separately at 5′ end via EDC/sulfo-NHS covalent coupling method (Kievit et al., 2012; Ong et al., 2017; Talan et al., 2018). The biophysical characterization was done after each step of synthesis, coating, and labeling with peptides by UV–Vis spectroscopy, Dynamic Light Scattering (DLS), Fourier Transform Infrared Spectroscopy (FT-IR), and Transmission Electron Microscopy (TEM). uPAR-specific targeting studies were done by FACS, cell adhesion, fluorescence microscope. Cell viability was assessed by (3-(4,5-Dimethylthiazol-2-yl)-2,5-Diphenyltetrazolium Bromide) MTT assay. The proposed hypothesis conferred that AuNPs/chitosan/GFD+SMB nanoconjugate exclusively bind and internalized by uPAR-overexpressing cells more efficiently than AuNPs/chitosan/GFD or AuNPs/chitosan/SMB alone. Thus, the developed nanoconjugate can be used to develop robust imaging tool for targeting of the uPAR receptor with significant potential in biomedical applications.

2. Material and methods

2.1. Reagents

Tetrachloroauric (III) acid (99.9% w/w) and chitosan extrapure (low molecular weight), monosodium phosphate, disodium phosphate, tris base, glycine, hydrochloric acid, nitric acid, sodium chloride, glacial acetic acid, sodium hydroxide were of analytical grade, and were purchased from Sigma-Aldrich Company (Delhi, India). Dulbecco's Phosphate-Buffered Saline (DPBS), Dulbecco's modified Eagle medium (DMEM), penicillin, streptomycin, and 0.25% trypsin-EDTA were purchased from Gibco Laboratories (India). Bovine fetal bovine serum (FBS) was purchased from Himedia Laboratories (India). Nunc microtiter plates 96 well were procured from Nunc, India. Trisodium citrate dehydrate was purchased from Sisco Research Laboratories (Delhi, India). Ovarian cancer cell line (SKOV3) was a kind gift from CSIR-IICB, Kolkata. All experiments were performed three times independently.

2.2. In-silico analysis

uPAR targeting peptides, GFD with molecular weight 4609.14 Da and SMB with molecular weight 5529.06 Da were found using a bioinformatics tool Protein Information Resource (PIR). Peptides were found in National Center for Biotechnology Information (NCBI) and aligned using ClustalW. In ClustalW, FASTA format of the peptides was obtained from NCBI, copied and entered in the section provided to paste sequences for alignment. Then, multiple alignment searches were performed. The score obtained in ClustalW was compared, and analyzed. The sequences obtained for human origin were compared using FASTA and Basic Local Alignment Search Tool (BLAST). The selected peptide of SMB and GFD were studied for structural compatibility and interaction analysis with uPAR. 3D structure of peptides generated through de novo approach PEP-FOLD online server (Lamiable et al., 2016). Protein structure of uPAR (1YWH) receptor downloaded from RCSB protein Data Bank (https://www.rcsb.org/) in PDB format. The docking studies of Protein-Peptide (Kumar, Sood, Tomar, & Chandra, 2019) performed using ClusPro 2.0 server (Kozakov et al., 2017). Protein complex visualization and hydrogen bonds and root-mean-square deviation (RMSD) value were calculated through University of California, San Francisco (UCSF) chimera (Goddard, Huang, & Ferrin, 2005) and Pymol (Lill & Danielson, 2011) visualization tool and LIGPLOT software (Wallace, Laskowski, & Thornton, 1995) used for verify the authentic hydrogen bonds.

2.3. Peptide synthesis and characterization

Peptides (GFD and SMB) were chemically synthesized using Fmoc (9-fluorenylmethoxy carbonyl) chemistry (Bartczak & Kanaras, 2011; Fields, 2001; Almeida et al., 2019). Fmoc amino acids were obtained from Lifetein LLC (New Jersey, USA). The peptide resins were

synthesized from the carboxyl terminus to the Lys amino terminus. This Fmoc-Lys-OH resin was incubated with dichloromethane (DCM) for 30 min, and washed twice with CH_2Cl_2 followed with dimethylformamide (DMF). The loaded peptide resin was then subjected to Fmoc-deprotection and amino acid coupling to build the rest of the peptide. Deprotection steps were performed by treatment with piperidine-DMF mixture and then washed with DMF, three times, to remove the deprotection buffer. Then, Fmoc-Glu-OH was coupled to the first amino acid to make GFD (VK-peptide) and finally DMF was removed. To make SMB peptide (DK-peptide), Fmoc-Thr-OH was used as the second amino acid, coupling and purification procedure were same as for VK-peptide. After each coupling step, the synthesized peptides were ninhydrin tested; further coupling and subsequent washing was repeated until the crude peptides were completely synthesized. After chain assembly i.e. coupling of the last amino acid, the synthesized crude peptides were cleaved from resin by treating with 20% piperidine in DMF. Deprotection of peptide was done by treating the resin with trifluoroacetic acid (TFA). Following precipitation in cold diethyl ether, crude peptide was collected by centrifugation and washed with further cold ether to remove scavengers. Peptides was then dissolved in 50% aqueous acetonitrile 0.07% TFA buffer and purified by preparative RP-HPLC. Fractions of greater than 95% purity were used for this study. The purity and molecular weight of the respective peptides were confirmed by MS. Peptides characterization were done using chromatographic technique i.e. reversed phase-HPLC (C18 HPLC column (Prodigy ODS3, 25 3200 mm; Phenomenex)) and MALDI-TOF-MS (PerSeptive Biosystems MALDI-TOF Voyager DE-RP Mass Spectrometer) to check the purity and appropriate size of the biomolecules. The synthesized peptide sequences of GFD and SMB were then labeled with a fluorescence molecule i.e. FITC.

2.4. AuNPs synthesis

AuNPs were synthesized by citrate reduction method (Kasoju, Shahdeo, et al., 2020; Gandhi et al., 2018). Briefly, gold chloroauric acid ($HAuCl_4$) was used as a salt, and trisodium citrate was used as a reducing agent. 100 μL of 10% $HAuCl_4$ was added to 100 mL of deionized water and boiled till 100 °C under continuous stirring. Different concentrations of sodium citrate (4% to 12% v/v) were added to find out the effect of citrate concentration on the size of AuNPs.

2.5. Stabilization of AuNPs with chitosan

AuNPs particles were coated with chitosan polymer as citrate reduced gold nanoparticles have a tendency to aggregate. For this, chitosan was prepared in 2% [v/v] glacial acetic acid, stirred continuously for 5–7 h at 34 °C and pH was maintained at 5.6 by sodium hydroxide and diluted with deionized water in 1:1 ratio (Du, Chen, Song, Li, & Chen, 2008; Kievit et al., 2012). Prior to coating of AuNPs with chitosan, the polymer was characterized through DLS (zeta potential) and FT-IR spectroscopy. Different molar ratios of AuNPs:chitosan, where one part of AuNPs and different parts of chitosan were used for coating (1:10, 1:20, 1:30, 1:40, and 1:50) were used for coating and sonicated for 60 min at 45 °C.

2.6. Functionalization of peptides with AuNPs/chitosan

Peptides were functionalised with chitosan coated AuNPs by carbodiimide activation (Singh et al., 2018; Yan, Zheng, Jiang, Li, & Xiao, 2015). A stock solution of both peptide ligands were prepared by dispersing GFD-FITC and SMB-FITC in deionized water and stored in dark conditions. The resultant 1 mg/mL solution was filtered using 0.2 μm filters and kept as aliquots at −20 °C. Four different concentration of peptides (0.5, 1.0, 1.5, and 2.0 μg/mL) were used to obtain desired nanoconjugate complex (AuNPs/chitosan/peptide) and the reaction was carried out at 4 °C in a dark room overnight (O/N).

2.7. Effect of pH on the stability of nanoconjugate

The effect of pH on the stability of the nanoconjugates was assessed at three different pH (3.0, 7.4, and 11.0). The buffers used for these experiments were glycine-HCl (pH 3.0), phosphate buffer (PB) (pH 7.4), and CB (pH 11.0). The glycine-HCl (pH 3.0) buffer was prepared by addition of 38 mg of glycine in (4 mL) distilled water and pH was adjusted by drop wise addition of HCL, phosphate buffer (PB) (pH 7.4) was prepared by addition of (0.10 g) Na_2HPO_4 and (0.17 mg) NaH_2PO_4 in (4 mL) of distilled water and desired pH (7.4) was maintained using HCL and NaOH. Final volume of 5 mL was adjusted by addition of distilled water, and Carbonate-bicarbonate (CB) buffer (pH 11.0) was prepared by addition of (0.52 mg) of $NaHCO_3$ and (0.46 mg) of Na_2CO_3 in (4 mL) distilled water and the volume was adjusted to 5 mL. The peptides were resuspended in different pH separately and conjugated with AuNPs/chitosan and further characterized to evaluate the optimum pH for its better stability.

2.8. Biophysical characterization

AuNPs, AuNPs/chitosan, AuNPs/chitosan/peptides (GFD/SMB) spectra were taken in the range of 400–1100 nm using a single beam UV–Vis spectroscopy. The hydrodynamic diameter and zeta potential was determined by DLS using particle sizing system equipped with a green laser excitation source operating at 532 nm/50 mW. A frequency of the photon counting was set at 200 kHz, while a scattering angle was fixed at 90°. Nanoconjugates were also characterized to confirm the presence of functional groups before and after polymer coating of AuNPs and analyzed by Ominic FT-IR software. Fluorescence spectra of the AuNPs, AuNPs/chitosan, AuNPs/chitosan/peptides (GFD/SMB) were taken in the range of 400–600 nm. TEM grids were prepared by drop casting 10 μL of AuNPs, AuNPs/chitosan, and air dried to observe the monodispersity. TEM imaging was done at 200 kV, and analyzed using ImageJ software.

2.9. In-vitro screening of uPAR specific SMB and GFD peptides

2.9.1. Cell culture
Skov3 cell lines were maintained in DMEM media, supplemented with 10% FBS, 1% P/S at 5% CO_2 at 37 °C. Confluent monolayer cells were subcultured by trypsinizing with 0.25% Trypsin-EDTA (TE) and centrifuged at 1500 rpm for 5 min. The cell pellet was washed with sterile PBS (pH 7.4) and resuspended in fresh media for further experiments.

2.9.2. Internalization of peptides
Skov3 (5000 cells/mL) were cultured in a 96 well plate. Cells were treated with AuNPs, AuNPs/chitosan, AuNPs/chitosan/GFD, AuNPs/chitosan/SMB, AuNPs/chitosan/GFD+SMB at 1, 0.5, and 0.25 μg/mL and incubated for 24 h at 37 °C, 5% CO_2. Cells were washed 3–4 times to remove any residue of nanoconjugates, resuspended in 1× PBS, and digested with TE. The fluorescence spectra were recorded at Ex/Em wavelength of 488/519 nm in a black plate using multimode ELISA reader.

2.9.3. Cell adhesion assay
For cell adhesion assay, 96 well plates were coated with Vn (5 μg/mL) and incubated O/N at 37 °C. 10,000 cells/well were plated (Skov3 cells) and allowed to adhere to Vn for 2 h. Blocking was done to minimize the non-specific cell binding to the E-plate by incubating all wells with 100 μL of 0.1% BSA at 37 °C for 1 h followed by washing twice with 150 μL 1× PBS. The targeting efficiency of nanoconjugates (AuNPs, AuNPs/chitosan, AuNPs/chitosan/GFD, AuNPs/chitosan/SMB, AuNPs/chitosan/GFD+SMB) was analyzed up to 5 h using xCELLigence RTCA instrument.

2.9.4. Fluorescence-activated cell sorting (FACS)

To test the binding affinity of nanoconjugates specific to uPAR, Skov3 cells (5×10^5 cells/well) were maintained at 37 °C in 5% CO_2 in DMEM media containing 10% FBS and 1% antibiotic (P/S). Different nanoconjugate treatments (AuNPs, AuNPs/chitosan, AuNPs/chitosan/GFD, AuNPs/chitosan/SMB, AuNPs/chitosan/SMB+GFD) were given separately at 1 μg/mL. After 2 h of treatment at 4 °C, cells were washed three times with PBS and subjected to FACS analysis using a BD/FACS Aria flow cytometer. Untreated cells were used to set the appropriate gates, after gating on viable cells, 20,000 events were acquired for each treatment. The results were analyzed using Flowjo software.

2.9.5. Fluorescence microscopy

Skov3 cells (5×10^4 cells/well) were cultured on collagen (Sigma) pre-coated coverglass slides and allowed to grow until semi-confluence. Cells were treated with different nanoconjugates (1 μg/mL) as described above in Section 2.9.1 for 4 h, washed thrice with PBS for 5 min, and fixed with 4% paraformaldehyde for 30 min at 4 °C. Blocking was performed with 2% bovine serum albumin and 2% goat serum in PBS for 15 min at RT (room temperature). Nuclei were stained with DAPI for 15 min at RT, washed twice with PBS. Images were acquired at 40× at 1024×1024 pixel resolution and further analyzed with ZEN software.
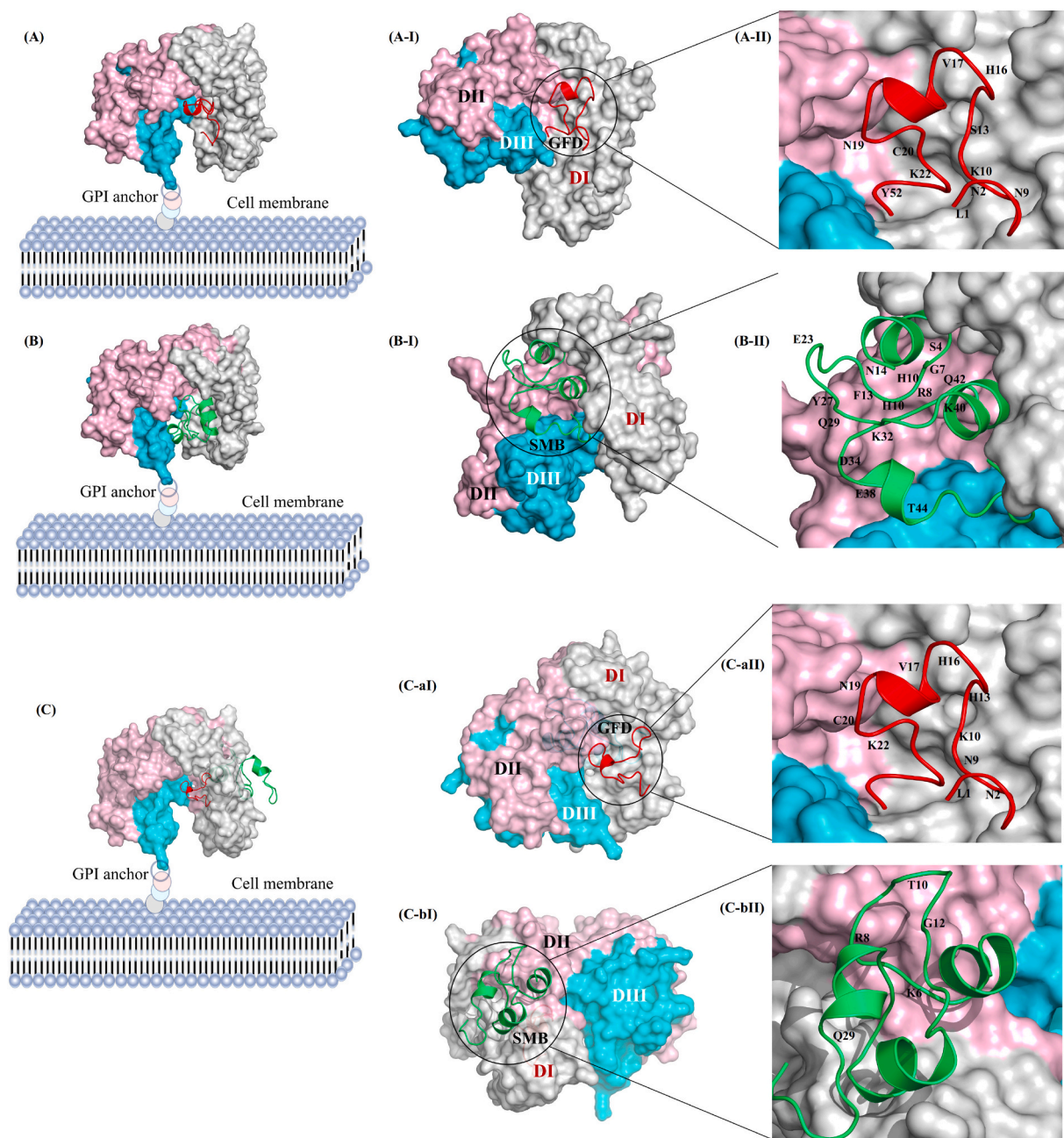

Fig. 1. Docking of urokinase plasminogen activator receptor (uPAR) with specific targeting peptide GFD and SMB. (A) Surface model of GPI anchored uPAR receptor with GFD peptide. (A-I) Binding of targeting peptide (GFD) (red ribbon model) in uPAR cavity domain DI (grey). (A-II) The GFD peptide directly interacting with the central cavity of uPAR domain I. (B) Surface model of uPAR receptor interacting with SMB peptide. (BI) Binding of targeting SMB peptide with domain II (light pink) of uPAR receptor. (BII) The SMB peptide (lime-green ribbon model) directly interacting in the central cavity of uPAR domain II. (C) Surface model of uPAR with both the peptides (GFD and SMB). (C-aI, C-bI) Interaction of two different peptides with different domains of uPAR. (C-aII, C-bII) The peptide circled narrowed the opening of the central cavity with different amino acid residues of GFD and SMB, simultaneously.

2.9.6. Cell viability

Skov3 cells (10,000 cells/well) were cultured in a 96 welled plates until sub-confluence and incubated at 37 °C, 5% CO$_2$ O/N. Cells were treated with (AuNPs, AuNPs/chitosan, AuNPs/chitosan/GFD, AuNPs/chitosan/SMB, AuNPs/chitosan/GFD+SMB) at concentrations ranging from 1.0 to 0.25 µg/mL for 24 and 48 h. Cells were washed twice with PBS and 10% of the culture media volume of (4,5-dimethyl-2-thiazolyl)-2,5-diphenyl-2H-tetrazolium bromide (MTT) was added and incubated for 4 h till the formazan crystals formation. 100 µL/well of solubilizing buffer was added to each and optical density of the wells was measured at 570 nm and a reference wavelength of 630 nm. The assay was performed in triplicate and the results were expressed as mean values ± standard deviation.

3. Results and discussion

Urokinase receptor, uPA, and Vitronectin are functionally linked and involved in the regulation of cell signaling, migration, and proliferation. Further, numerous studies have also reported receptor tenancy with uPA being key to interactions between uPAR and Vn. To access the functional stability of whole together protein, uPAR-GFD complex was further docked with SMB (binding affinity ≈ −623 kcal/mol) which was less than the individual docking studies of uPAR with GFD, and SMB. The docking studies exhibited a higher binding affinity when uPAR was docked individually with GFD, and SMB (−982.4 and −753.2 kcal/mol) with a RMSD value of 0.2 and 0.1. However, when uPAR-GFD complex was docked with SMB, the binding affinity was relatively less at −623 kcal/mol and a RMSD value of 0.3, with a significant conformational change and energy difference in the structure of uPAR/GFD/SMB complex (Fig. 1). Table S1 showed the detailed molecular docking and interaction analysis of GFD and SMB with uPAR, wherein, we have shown the free binding energy, number of hydrogen bonds, RMSD value, and hydrogen bond formation between uPAR and peptides at specific location (Fig. S1-a, b, and c). On the basis of above docking studies, we conclude that the designed peptides can efficiently be employed for targeting and imaging of uPAR in cancer diagnostics.

Therefore, biocompatible polymer coated AuNPs were successfully functionalized with fluorescently labeled peptides (GFD/SMB) for efficient targeting and imaging of uPAR-positive cancer cells (Ong et al., 2017). To attain efficient imaging and targeting of uPAR- overexpressing cells, sequence of GFD and SMB were synthesized using Fmoc method and N terminus of the peptides were labeled with FITC. Peptides (GFD and SMB) purification was done using HPLC (Fig. S2-a, and b) which further confirmed a single peak with a purity of 99.98% and molecular mass of 4609.14 Da for GFD and 5529.06 Da for SMB, which was similar to the expected molecular weight. The synthesized peptides were covalently attached with carboxyl group via EDC/sulfo-NHS carbodiimide activation method (Fig. 2) with amine functionalized (NH$_2$-) chitosan stabilized AuNPs.

Monodispersed AuNPs (20 nm) were prepared by citrate reduction method with gold chloride as a precursor and sodium citrate as the reducing agent (Talan et al., 2018). For this, variable concentrations of sodium citrate (4, 6, 8, 10, and 12%) were used, with fixed concentration of gold chloride (Fig. S3). Addition of citrate to the gold chloride solution resulted in a gradual conversion of color from violet to red wine thereby confirming the successful synthesis of AuNPs. Resultant AuNPs were characterized with UV–Vis spectroscopy that showed a red shift in plasmon peak from 520 to 530 nm (from 4% to 12% of sodium citrate). The final synthesis was done with 4% sodium citrate with surface plasmon peak at 520 nm. The zeta potential of chitosan polymer was +52.6 mV (Fig. S4.a), which indicated the positive charge on the surface of chitosan polymer. FT-IR investigation showed stretching vibration in the range of 3400–3200 cm^{-1} corresponding to N—H and O—H stretching. Major transmittance bands were observed between 2123 and 1200 cm^{-1}, which mainly attributed to amine group of chitosan. The peak at 1644 cm^{-1} indicated the N—H bending. Medium peak at 1393 and 1279.60 cm^{-1} showed OH bending of acetic acid which was used to dissolve the chitosan and C—N stretching of primary amine (Fig. S4.b).

To further, optimize the concentration of chitosan coating, different molar ratios of chitosan to the fixed volume of AuNPs were taken (1:10, 1:20, 1:30, 1:40, 1:50) and characterized with UV–Vis spectroscopy and hydrodynamic diameter (Fig. S5. a & b). A bathochromic shift of 10 nm was noted at 1:10 M ratio confirmed the coating of chitosan on the surface of AuNPs (Table S5. c).

Herein, GFD/SMB peptides were spaced by a chitosan polymer containing amine groups that favor the formation of continuous
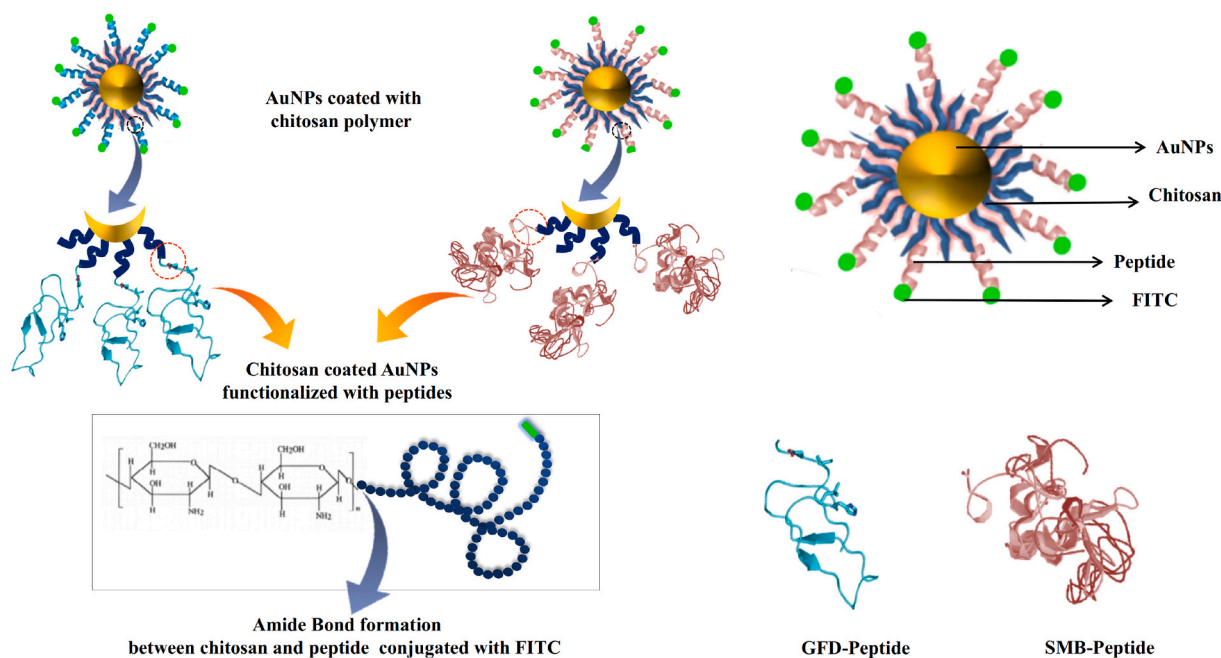

Fig. 2. Schematic representation of GFD/SMB peptide-functionalized with chitosan coated AuNPs. Square box shows the chitosan structure linked with peptide sequence via amide bond formation.

passivation layer around AuNPs. The higher surface density of chitosan chains promoted minimal protein adsorption and nonspecific interactions thereby providing optimal colloidal stability with the hydrodynamic diameter (20 nm) and charge (−33 mV) of AuNPs (Clogston & Patri, 2011). Moreover, post coating with chitosan polymer, the hydrodynamic diameter was seen to increase from ±20 nm to ±50 nm, along with a shift in charge from −33 ± 6.1 mV to +37 ± 7.0 mV. Additionally, chitosan stabilized AuNPs were functionalized with FITC labeled peptides GFD and SMB via carbodiimide chemistry. Addition of peptides onto the surface of AuNPs resulted in further red shift from ~530 nm to ~540 nm (Fig. 3b), which was also accompanied by an increase in the hydrodynamic diameter (±150), zeta potential (~+44 ± 3.6 mV), and polydispersity index (0.2–0.3). Monodispersed AuNPs with core size of 20 ± 5 nm were synthesized, where polymer coating could be observed in the form of deposition around the AuNPs (Fig. 3e-ii). The functional groups of AuNPs and AuNPs/chitosan were assessed by FT-IR to confirm the coating of polymer (Fig. 3f) with a spectra at 3450 cm^{-1} corresponds to O—H stretching, stretch of C=O at 1638 cm^{-1} for the carbonyl, while the spectra at 1281 cm^{-1} depicts the C—N stretching of primary amine group, 1364 cm^{-1}, 1422 cm^{-1}, 1552 cm^{-1},

corresponding to O—H bending of CH$_2$.OH, CH.OH, N—H, respectively, further corroborated the coating of AuNPs with chitosan. In Table 1, representative characteristics of AuNPs functionalized with polymer and peptide are summarized.

Several studies have reported the relevancy of ligand:shell

Table 1
Characterization of AuNPs/chitosan/GFD/SMB peptide by UV–Vis Spectroscopy, Dynamic Light Scattering (DLS), Polydispersity Index and ζ-Potential.

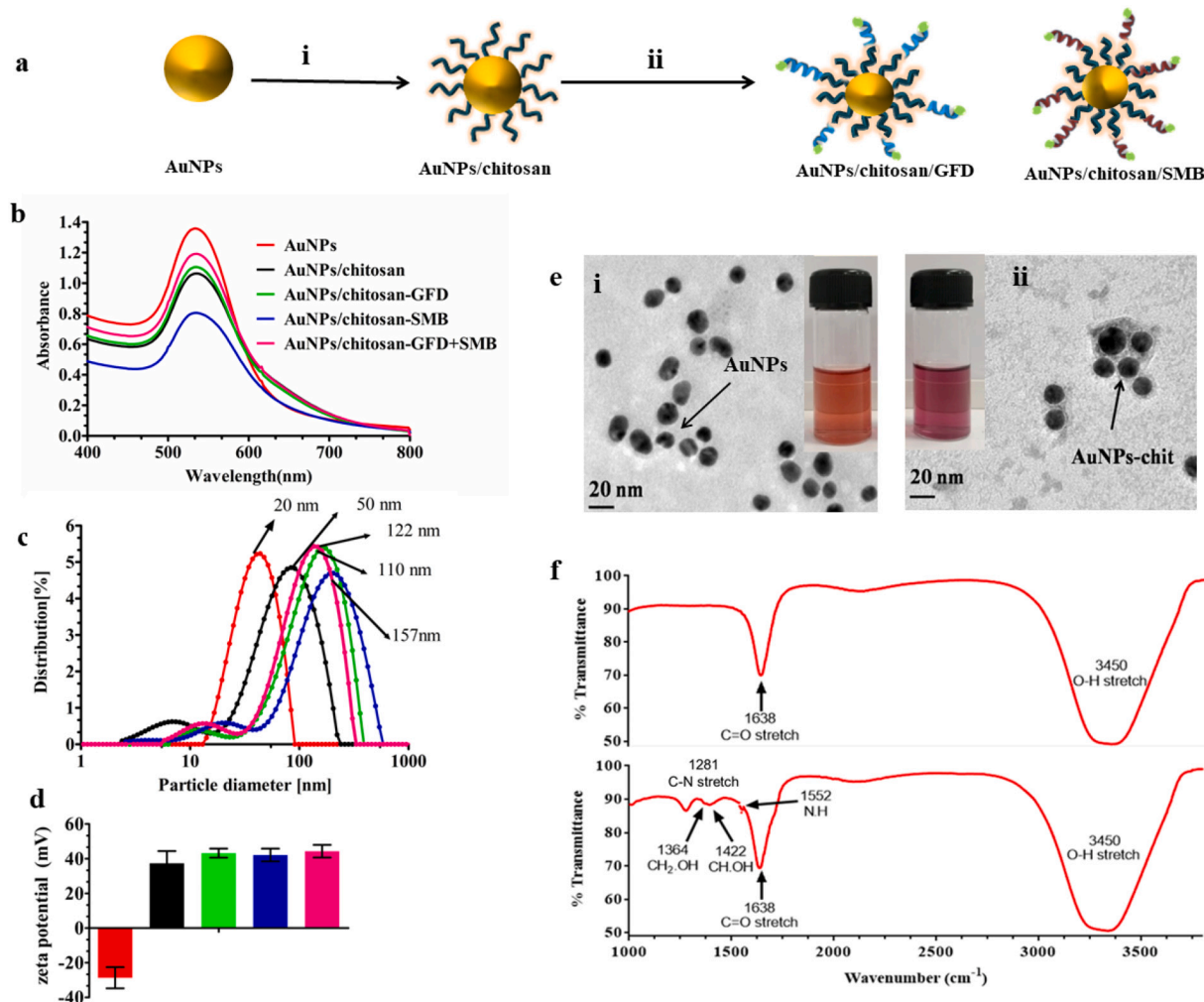| Formulations	SPR (nm)	DLS (nm)	Polydispersity index	Zeta potential (mV)
AuNPs	520	20 ± 5	0.2	−33 ± 6.1
AuNPs/chitosan	530	50 ± 5	0.2	+37 ± 7.0
AuNPs/chitosan/GFD	536	120 ± 2	0.2	+43 ± 2.6
AuNPs/chitosan/SMB	538	155 ± 5	0.28	+42 ± 3.6
AuNPs/chitosan/GFD+SMB	540	110 ± 5	0.2	+44 ± 3.6

Fig. 3. (a) Synthesis, and functionalization of gold nanoparticles (AuNPs), followed by coating with chitosan to flank free amino groups (NH$_2$-) and conjugation with carboxyl groups (-COO$^-$) of peptide ligands (GFD and SMB); Biophysical characterization of surface modified AuNPs conjugated with chitosan and peptides. (b) UV–Vis spectroscopy with the red shift of 3–5 nm if compared with AuNPs, and AuNPs/chitosan, AuNPs/chitosan/GFD and AuNPs/chitosan/SMB. (c) DLS spectra of AuNPs, AuNPs/chitosan, AuNPs/chitosan/GFD, AuNPs/chitosan/SMB and AuNPs/chitosan/GFD+SMB showed change in hydrodynamic diameters of 20 nm, 50 nm, 110 nm, 157 nm and, 122 nm respectively. (d) Zeta potential of AuNPs, AuNPs/chitosan, AuNPs/chitosan/GFD, AuNPs/chitosan/SMB and AuNPs/chitosan/GFD+SMB as determined by DLS. (e) TEM micrograph of (i) AuNPs and (ii) AuNPs/chitosan confirms the monodispersed AuNPs of 20 ± 5 nm diameter with a uniform layer of chitosan on nanoparticles surface. (f) FTIR spectra of (i) AuNPs and (ii) AuNPs/chitosan shows a stretch of C=O at 1638 cm^{-1} in both cases to confirm the presence of carboxyl groups, while the stretch at 1281 cm^{-1}, 1364 cm^{-1}, 1422 cm^{-1}, 1552 cm^{-1} corresponds to C—N, CH$_2$.OH, CH.OH, and N.H groups.

composition and ligand density on AuNPs surface to their targeting efficacy and particle internalization mechanism. Therefore, chitosan functionalized AuNPs were optimized at different concentrations of peptides (optimum concentration at 1.0 μg/mL as shown in Fig. S6 and pH range of 3.0 to 11.0 with optimum concentration at 7.4) and thereafter, the nanocomplexes were aggregated (Fig. S7).

The biological activity of AuNPs and its conjugates were assessed in uPAR-positive, human Skov3 cancer cells. A significant uptake of AuNPs/chitosan/GFD+SMB was marked as followed by AuNPs/chitosan/GFD, while a lower degree of internalization was noted in case of AuNPs/chitosan/SMB complex (Fig. 4a). Further, it was also observed that, contrary to AuNPs/chitosan/SMB, increase in the concentration of treatment from 0.25 μg/mL to 1 μg/mL resulted in an increased uptake in case AuNPs/chitosan/GFD+SMB and AuNPs/chitosan/GFD (Fig. 4b). To assess the extent of receptor-mediated endocytosis, the binding efficiency of each nanoconjugates (AuNPs, AuNPs/chitosan/GFD, AuNPs/chitosan/SMB, AuNPs/chitosan/GFD+SMB was examined by FACS as a function of internalized particles. Cell-associated fluorescence (by FITC) was observed after 2 h of incubation of each nanoconjugate with Skov3 cells at 4 °C. The maximum binding was exhibited by AuNPs/chitosan/GFD+SMB, followed by AuNPs/chitosan/GFD and AuNPs/chitosan/SMB (Fig. 4c). Cell adhesion assay also correlated with FACS findings and hinted towards an active involvement of receptor-mediated targeting in case of GFD+SMB>GFD, while negligible internalization was evident with non-targeted SMB, AuNPs, and AuNPs/chitosan was added for the treatment (Fig. 4d). The above data suggested that binding of AuNPs/chitosan/GFD peptide nanoconjugates was necessary for allosteric modulation of uPAR receptor which is a pre-requisite for binding of AuNPs/chitosan/SMB peptide nanoconjugates for efficient cellular uptake in uPAR positive Skov3 cancer cells.

FACS is a powerful tool for the quantification of associated targeting of nanoconjugates with cells, unfortunately it does not differentiate between cellular binding and cellular internalization. However, the confirmation of uptake internalization events of nanoconjugates can be performed by fluorescence microscopy. To affirm cellular uptake and internalization events of nanoconjugates by Skov3 cells, we conducted fluorescence microscopy experiments. Fig. 5 displays the uptake and internalization of AuNPs/chitosan/GFD, AuNPs/chitosan/SMB, AuNPs/chitosan/GFD+SMB nanoconjugate complex. The active involvement of a receptor-mediated targeting in case of AuNPs/chitosan/GFD+SMB and AuNPs/chitosan/GFD nanoconjugate complex was observed inside the cell. Negligible internalization was evident with non-targeted AuNPs/chitosan/SMB (Fig. 5a).

In order to assess the cell viability, the target Skov3 cells were incubated with nanoconjugate (1 μg/mL, 0.5 μg/mL, 0.25 μg/mL) for 24 and 48 h and the cytotoxicity study was performed with conventional MTT (4, 5-dimethyl-2-thiazolyl)-2, 5-diphenyl-2H-tetrazolium bromide) assay that relies on color change of MTT by mitochondrial succinate dehydrogenase. There was maximum cytotoxicity observed in Skov3 cells treated with the AuNPs/chitosan/GFD+SMB > GFD > SMB at 24 h (Fig. 5b-i) that enhanced after a prolonged incubation period of 48 h at a dosage of 1.0 μg/mL of nanoconjugates (Fig. 5b-ii). While AuNPs and AuNPs/chitosan treated cells demonstrated negligible cytotoxicity in both cases (24 h and 48 h). Thus, this result substantiates the fact that high cytotoxicity of nanoconjugate towards Skov3 cells originates from their specificity towards targeting of uPAR-overexpressing cells, only.

4. Conclusions

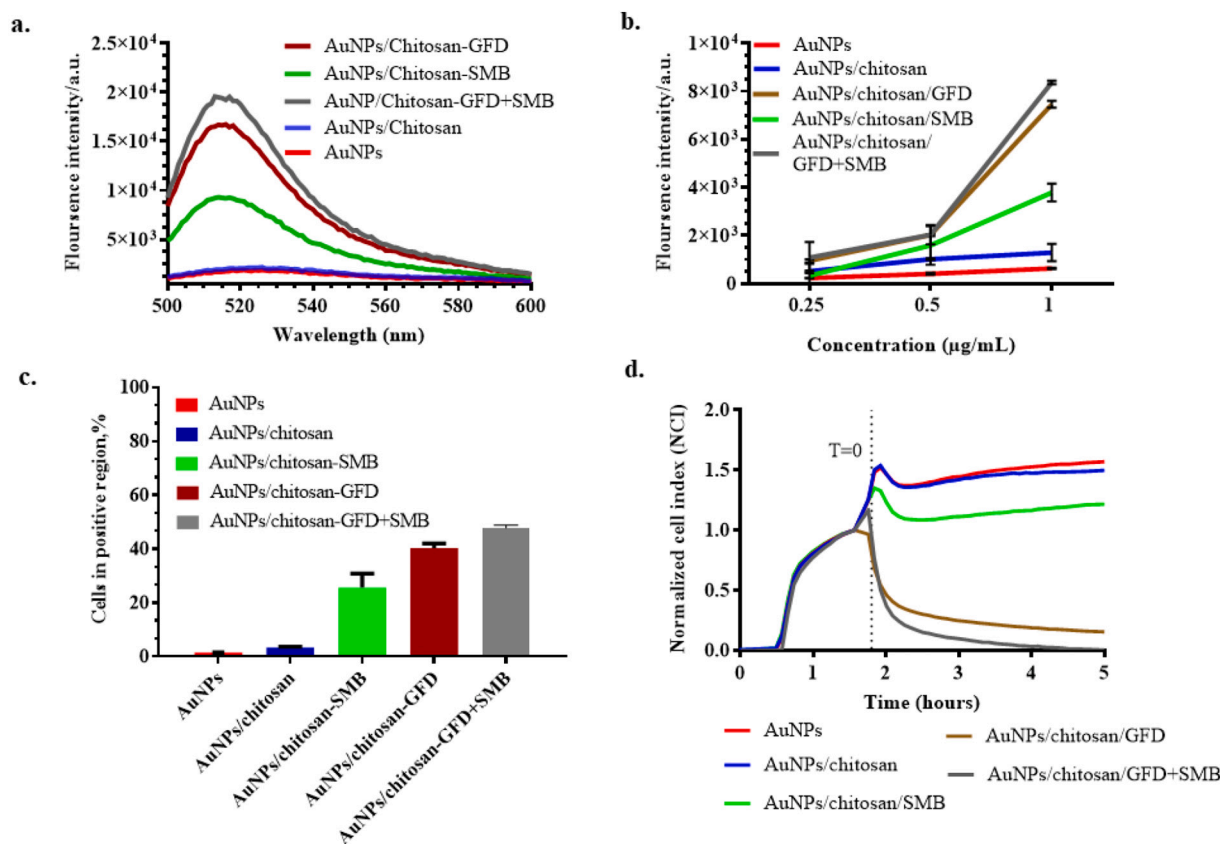In this study, we have presented a promisingly potent imaging

Fig. 4. In-vitro targeting assay (a) fluorescence spectra of different treatments of the nanoconjugates. (b) Comparison of the cellular uptake of different nanoconjugates at variable concentration. (c) FACS analysis of uPAR targeting nanoconjugates on Skov3 cells. Cells were incubated for 2 h with 1 μg/mL of nanoconjugates, which indicate the higher uptake of AuNPs/chitosan/GFD+SMB. (d) Cell adhesion assay- cells were treated after 2 h and the effect was recorded with the different nanoconjugates up to 5 h.
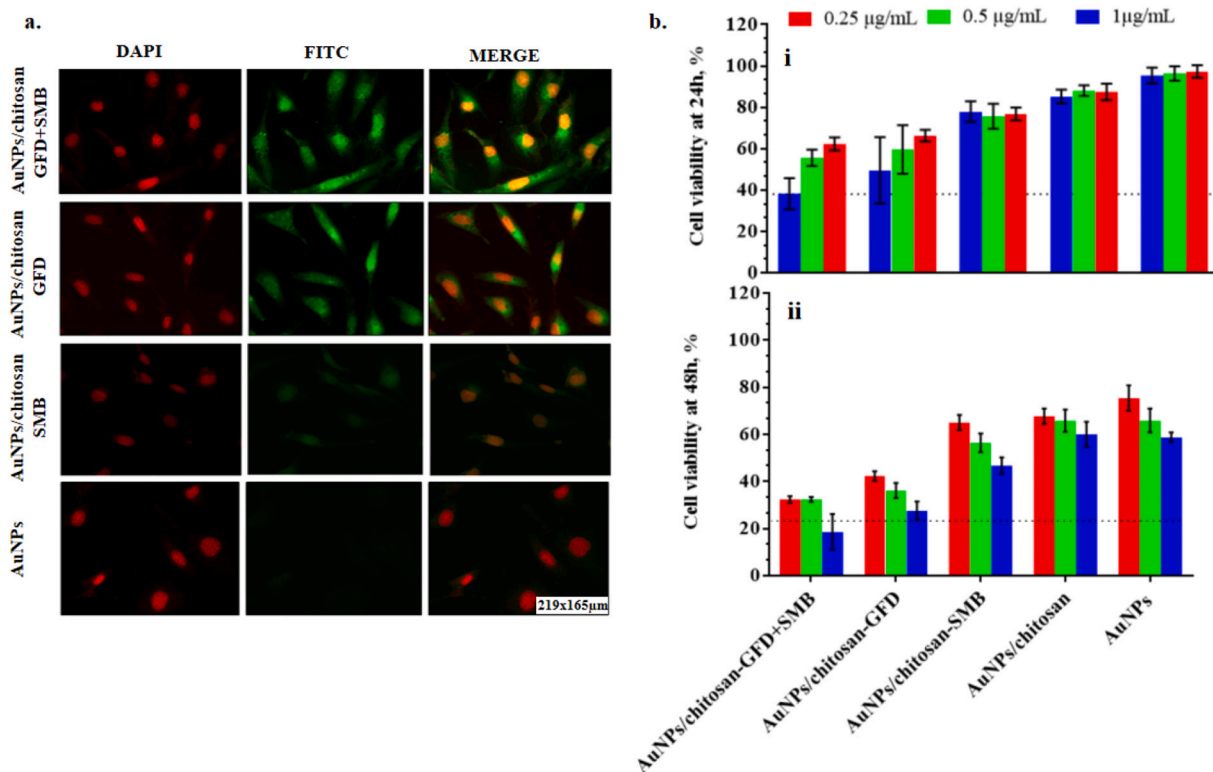
Fig. 5. (a) Fluorescent microscopy study of uPAR targeting with nanoconjugates and control on Skov3 cells (uPAR+). Nuclei were stained DAPI (red). Scale bar corresponds to 219.7 μm × 165.75 μm. (b) Cell viability assay with MTT. Skov3 cells were treated with nanoconjugates (0.25, 0.5, and 1 μg/mL) for up to 24 h and 48 h. The results are expressed as mean values ± SE of three individual experiments. Untreated cells are shown as negative control.

approach for bioconjugation of uPAR-specific peptides functionalized with AuNPs coated with polymer for efficient and selective targeting of cancer cells. The peptides derived from the GFD domain of uPA and SMB domain of vitronectin have been established to play a central role in their binding to uPAR due to receptor allosteric modulation. Herein, we have functionalized AuNPs with uPAR-specific peptides that mimic the sequence of GFD and SMB and play a vital role in efficient targeting and imaging of ovarian cancer. It has been further delineated that these peptide-nanoconjugates promoted receptor selectivity via increased cellular uptake and internalization of uPAR-overexpressing cells. The proposed hypothesis proved by showing the binding affinity of GFD and SMB peptides for the specific uPAR receptor by uptake assay with fluorescence spectroscopy, cell adhesion, flow cytometry, and fluorescence imaging that showed higher binding affinity of GFD+SMB peptides together over GFD or SMB peptide alone with uPAR, making them a suitable target. Therefore, uPAR-targeted nanoconjugates represent themselves as a cogent means for specific and selective targeting of uPAR in cancer imaging.

CRediT authorship contribution statement

Deepshikha Shahdeo- performed the experiment, Veerbhan Kesarwani- performed the in-silico experiments, Deepa Suhag- writing and discussion of the manuscript, Jahangeer Ahmed and Saad M Alshehri-writing, discussion and revision of the manuscript, Sonu Gandhi-designing the experiments, writing the manuscript.

Declaration of competing interest

There is no conflict of interest among the authors.

Appendix A. Supplementary data

Supplementary data to this article can be found online at https://doi.org/10.1016/j.carbpol.2021.118138.

References

Almeida, N. R. D., Han, Y., Perez, J., Kirkpatrick, S., Wang, Y., & Sheridan, M. C. (2019). Design, synthesis, and nanostructure-dependent antibacterial activity of cationic peptide amphiphiles. *ACS Applied Materials and Interfaces, 11*(3), 2790–2801. https://doi.org/10.1021/acsami.8b17808

Andreasen, P. A., Egelund, R., & Petersen, H. H. (2000). The plasminogen activation system in tumor growth, invasion, and metastasis. *Cellular and Molecular Life Sciences, 57*(1), 25–40. https://doi.org/10.1007/s000180050497

Ansari, M. J., Anwer, M. K., Jamil, S., Al-Shdefat, R., Ali, B. E., Ahmad, M. M., & Ansari, M. N. (2016). Enhanced oral bioavailability of insulin-loaded solid lipid nanoparticles: Pharmacokinetic bioavailability of insulin-loaded solid lipid nanoparticles in diabetic rats. *Drug Delivery, 23*(6), 1972–1979. https://doi.org/10.3109/10717544.2015.1039666

Avvakumova, S., Galbiati, E., Pandolfi, L., Mazzucchelli, S., Cassani, M., Gori, A., Longhi, R., & Prosperi, D. (2014). Development of U11-functionalized gold nanoparticles for selective targeting of urokinase plasminogen activator receptor-positive breast cancer cells. *Bioconjugate Chemistry, 25*(8), 1381–1386. https://doi.org/10.1021/bc500202b

Bachran, C., & Leppla, S. H. (2016). Tumor targeting and drug delivery by anthrax toxin. *Toxins (Basel), 8*(7), 97. https://doi.org/10.3390/toxins8070197

Bartczak, D., & Kanaras, A. G. (2011). Preparation of peptide-functionalized gold nanoparticles using one pot EDC/Sulfo-NHS coupling. *Langmuir., 27*(16), 10119–10123. https://doi.org/10.1021/la2022177

Caracciolo, G., Cardarelli, F., Pozzi, D., Salomone, F., Maccari, G., Bardi, G., … Laganà, A. (2013). Selective targeting capability acquired with a protein corona adsorbed on the surface of 1,2-dioleoyl-3-trimethylammonium propane/DNA nanoparticles. *ACS Applied Materials & Interfaces, 5*(24), 13171–13179. https://doi.org/10.1021/am404171h

Carriero, M. V., Del Vecchio, S., Franco, P., Potena, M. I., Chiaradonna, F., Botti, G., … Salvatore, M. (1997). Vitronectin binding to urokinase receptor in human breast cancer. *Clinical Cancer Research, 3*(8), 1299–1308.

Chen, Z., Wang, Z., Chen, X., Xu, H., & Liu, J. (2013). Chitosan-capped gold nanoparticles for selective and colorimetric sensing of heparin. *Journal of Nanoparticle Research, 15*(9), 1930. https://doi.org/10.1007/s11051-013-1930-9

Chew, J. L., Wolfowicz, C. B., Mao, H. Q., Leong, K. W., & Chua, K. Y. (2003). Chitosan nanoparticles containing plasmid DNA encoding house dust mite allergen, Der p 1 for oral vaccination in mice. *Vaccine., 21*(21–22), 2720–2729. https://doi.org/10.1016/S0264-410X(03)00228-7

Chikkaveeraiah, B. V., Bhirde, A. A., Morgan, N. Y., Eden, H. S., & Chen, X. (2012). Electrochemical immunosensors for detection of cancer protein biomarkers. *ACS Nano, 6*(8), 6546–6561. https://doi.org/10.1021/nn3023969

Clogston, J. D., & Patri, A. K. (2011). Zeta potential measurement. In *Characterization of nanoparticles intended for drug delivery* (pp. 63–70). Humana Press. https://doi.org/10.1007/978-1-60327-198-1_6.

Du, D., Chen, S., Song, D., Li, H., & Chen, X. (2008). Development of acetylcholinesterase biosensor based on CdTe quantum dots/gold nanoparticles modified chitosan microspheres interface. *Biosensors & Bioelectronics, 24*(3), 475–479. https://doi.org/10.1016/j.bios.2008.05.005

Duan, T., Zhou, Z., Su, G., Liu, L., Guan, M., Du, B., & Zhang, Q. (2014). Chitosan-coated gold nanorods for cancer therapy combining chemical and photothermal effects. *Macromolecular Bioscience, 14*(8), 1160–1169. https://doi.org/10.1002/mabi.201300563

Duffy, M. J. (2004). The urokinase plasminogen activator system: Role in malignancy. *Current Pharmaceutical Design, 10*(1), 39–49. https://doi.org/10.2174/1381612043453559

Fedorova, A., Zobel, K., Gill, H. S., Ogasawara, A., Flores, J. E., Tinianow, J. N., … Deshayes, K. (2011). The development of peptide-based tools for the analysis of angiogenesis. *Chemistry & Biology, 18*(7), 839–845. https://doi.org/10.1016/j.chembiol.2011.05.011

Fields, G. B. (2001). Introduction to peptide synthesis. *Current Protocols in Protein Science, 26*(1). https://doi.org/10.1002/0471140864.ps1801s26 (18-1).

Gandhi, S., Arami, H., & Krishnan, K. M. (2016). Detection of cancer-specific proteases using magnetic relaxation of peptide-conjugated nanoparticles in biological environment. *Nano Letters, 16*(6), 3668–3674. https://doi.org/10.1021/acs.nanolett.6b00867

Gandhi, S., Banga, I., Maurya, P. K., & Eremin, S. A. (2018). Gold nanoparticles-single chain fragment variable antibody as immunoprobe for rapid detection of morphine by dipstick. *RSC Advances, 8*(3), 1511–1518. https://doi.org/10.1039/C7RA12810J

Goddard, T. D., Huang, C. C., & Ferrin, T. E. (2005). Software extensions to UCSF chimera for interactive visualization of large molecular assemblies. *Structure., 13*(3), 473–482. https://doi.org/10.1016/j.str.2005.01.006

Hettiarachchi, S. U., Prasai, B., & McCarley, R. L. (2014). Detection and cellular imaging of human cancer enzyme using a turn-on, wavelength-shiftable, self-immolative profluorophore. *Journal of the American Chemical Society, 136*(21), 7575–7578. https://doi.org/10.1021/ja5030707

Kalimuthu, K., Lubin, B.-C., Bazylevich, A., Gellerman, G., Shpilberg, O., Luboshits, G., & Firer, M. A. (2018). Gold nanoparticles stabilize peptide-drug-conjugates for sustained targeted drug delivery to cancer cells. *Journal of Nanobiotechnology, 16*(1), 34. https://doi.org/10.1186/s12951-018-0362-1

Kasoju, A., Shahdeo, D., Khan, A. A., Shrikrishna, N. S., Mahari, S., Alanazi, A. M., … Gandhi, S. (2020). Fabrication of microfluidic device for Aflatoxin M1 detection in milk samples with specific aptamers. *Scientific Reports, 10*(1), 4627. https://doi.org/10.1038/s41598-020-64241-8

Khanna, M., Wang, F., Jo, I., Knabe, W. E., Wilson, S. M., Li, L., … Meroueh, S. O. (2011). Targeting multiple conformations leads to small molecule inhibitors of the uPAR-uPA protein-protein interaction that block cancer cell invasion. *ACS Chemical Biology, 6*(11), 1232–1243. https://doi.org/10.1021/cb200180m

Kievit, F. M., Stephen, Z. R., Veiseh, O., Arami, H., Wang, T., Lai, V. P., … Zhang, M. (2012). Targeting of primary breast cancers and metastases in a transgenic mouse model using rationally designed multifunctional SPIONs. *ACS Nano, 6*(3), 2591–2601. https://doi.org/10.1021/nn205070h

Kjaergaard, M., Hansen, L. V., Jacobsen, B., Gardsvoll, H., & Ploug, M. (2008). Structure and ligand interactions of the urokinase receptor (uPAR). *Frontiers in Bioscience, 13*(5441), 61. https://doi.org/10.2741/3092

Kozakov, D., Hall, D. R., Xia, B., Porter, K. A., Padhorny, D., Yueh, C., Beglov, D., & Vajda, S. (2017). The ClusPro web server for protein-protein docking. *Nature Protocols, 12*(2), 255–278. https://doi.org/10.1038/nprot.2016.169

Kumar, N., Sood, D., Tomar, R., & Chandra, R. (2019). Antimicrobial peptide designing and optimization employing large-scale flexibility analysis of protein-peptide fragments. *ACS Omega, 4*(25), 21370–21380. https://doi.org/10.1021/acsomega.9b03035

Lamiable, A., Thévenet, P., Rey, J., Vavrusa, M., Derreumaux, P., & Tufféry, P. (2016). PEP-FOLD3: Faster de novo structure prediction for linear peptides in solution and in complex. *Nucleic Acids Research, 44*, 449–454. https://doi.org/10.1093/nar/gkw329

Lee, J. F. T. (2015). A short review on chitosan membrane for biomolecules immobilization. *Journal of Molecular and Genetic Medicine, 09*(178), 1–5. https://doi.org/10.4172/1747-0862.1000178

Lill, M. A., & Danielson, M. L. (2011). Computer-aided drug design platform using PyMOL. *Journal of Computer-Aided Molecular Design, 25*(1), 13–19. https://doi.org/10.1007/s10822-010-9395-8

MacDonald, T. J., DeClerck, Y. A., & Laug, W. E. (1998). Urokinase induces receptor mediated brain tumor cell migration and invasion. *Journal of Neuro-Oncology, 40*(3), 215–226. https://doi.org/10.1023/A:1006150506789

Madsen, C. D., Ferraris, G. M. S., Andolfo, A., Cunningham, O., & Sidenius, N. (2007). uPAR-induced cell adhesion and migration: Vitronectin provides the key. *The Journal of Cell Biology, 177*(5), 927–939. https://doi.org/10.1083/jcb.200612058

Magnussen, S. N., Hadler-Olsen, E., Costea, D. E., Berg, E., Jacobsen, C. C., Mortensen, B., … Svineng, G. (2017). Cleavage of the urokinase receptor (uPAR) on oral cancer cells: Regulation by transforming growth factor - β1 (TGF-β1) and potential effects on migration and invasion. *BMC Cancer, 17*(1), 350. https://doi.org/10.1186/s12885-017-3349-7

Mauro, C. D., Pesapane, A., Formisano, L., Rosa, R., D'Amato, V., Ciciola, P., Servetto, A., Marciano, R., Orsini, R. C., Monteleone, F., Zambrano, N., Fontanini, G., Servadio, A., Pignataro, G., Grumetto, L., Lavecchia, A., Bruzzese, D., Iaccarino, A., Troncone, G., … Bianco, R. (2017). Urokinase-type plasminogen activator receptor (uPAR) expression enhances invasion and metastasis in RAS mutated tumors. *Scientific Reports, 7*(1), 1–12. https://doi.org/10.1038/s41598-017-10062-1

Medley, C. D., Smith, J. E., Tang, Z., Wu, Y., Bamrungsap, S., & Tan, W. (2008). Gold nanoparticle-based colorimetric assay for the direct detection of cancerous cells. *Analytical Chemistry, 80*(4), 1067–1072. https://doi.org/10.1021/ac702037y

Mohammed, M. A., Syeda, J., Wasan, K. M., & Wasan, E. K. (2017). An overview of chitosan nanoparticles and its application in non-parenteral drug delivery. *Pharmaceutics, 9*(4), 53. https://doi.org/10.3390/pharmaceutics9040053

Molino, Y., David, M., Varini, K., Jabès, F., Gaudin, N., Fortoul, A., & Bakloul, K. (2017). Use of LDL receptor-targeting peptide vectors for in vitro and in vivo cargo transport across the blood-brain barrier. *The FASEB Journal, 31*(5), 1807–1827. https://doi.org/10.1096/fj.201600827R

Munhoz, L. S., Vargas, G. D., Fischer, G., de Lima, M., Esteves, P. A., & de O. Hübner, S. (2014). Avian IgY antibodies: Characteristics and applications in immunodiagnostic. *Ciência Rural, 44*(1), 153–160. https://doi.org/10.1590/S0103-84782014000100025

Nykjar, A. (1997). Recycling of the urokinase receptor upon internalization of the uPA: serpin complexes. *The EMBO Journal, 16*(10), 2610–2620. https://doi.org/10.1093/emboj/16.10.2610

Ong, Z. Y., Chen, S., Nabavi, E., Regoutz, A., Payne, D. J., Elson, D. S., … Porter, A. E. (2017). Multibranched gold nanoparticles with intrinsic LAT-1 targeting capabilities for selective photothermal therapy of breast cancer. *ACS Applied Materials and Interfaces, 9*(45), 39259–39270. https://doi.org/10.1021/acsami.7b14851

Pavón, M. A., Arroyo-Solera, I., Céspedes, M. V., Casanova, I., León, X., & Mangues, R. (2016). uPA/uPAR and SERPINE1 in head and neck cancer: Role in tumor resistance, metastasis, prognosis and therapy. *Oncotarget, 7*(35), 57351–57366. https://doi.org/10.18632/oncotarget.10344

Ploug, M., Østergaard, S., Gårdsvoll, H., Kovalski, K., Holst-Hansen, C., Holm, A., … Danø, K. (2001). Peptide-derived antagonists of the urokinase receptor. Affinity maturation by combinatorial chemistry, identification of functional epitopes, and inhibitory effect on cancer cell intravasation. *Biochemistry, 40*(40), 12157–12168. https://doi.org/10.1021/bi010662g

Rakashanda, S., Rana, F., Rafiq, S., Masood, A., & Amin, S. (2012). Role of proteases in cancer: A review. *Biotechnology and Molecular Biology Reviews, 7*(4), 90–101. https://doi.org/10.5897/BMBR11.027

Rea, V. E. A., Lavecchia, A., Di Giovanni, C., Rossi, F. W., Gorrasi, A., Pesapane, A., … Montuori, N. (2013). Discovery of new small molecules targeting the vitronectin-binding site of the urokinase receptor that block cancer cell invasion. *Molecular Cancer Therapeutics, 12*(8), 1402–1416. https://doi.org/10.1158/1535-7163.MCT-12-1249

Roberts, A., Tripathi, P. P., & Gandhi, S. (2019). Graphene nanosheets as an electric mediator for ultrafast sensing of urokinase plasminogen activator receptor—A biomarker of cancer. *Biosensors & Bioelectronics, 141*. https://doi.org/10.1016/j.bios.2019.111398

Sidenius, N., Andolfo, A., Fesce, R., & Blasi, F. (2002). Urokinase regulates vitronectin binding by controlling urokinase receptor oligomerization. *The Journal of Biological Chemistry, 277*(31), 27982–27990. https://doi.org/10.1074/jbc.M111736200

Singh, S., Mishra, P., Banga, I., Parmar, A. S., Tripathi, P. P., & Gandhi, S. (2018). Chemiluminescence based immunoassay for the detection of heroin and its metabolites. *Bioimpacts, 8*(1), 53–58. https://doi.org/10.15171/bi.2018.07

Talan, A., Mishra, A., Eremin, S. A., Narang, J., Kumar, A., & Gandhi, S. (2018). Ultrasensitive electrochemical immuno-sensing platform based on gold nanoparticles triggering chlorpyrifos detection in fruits and vegetables. *Biosensors & Bioelectronics, 105*, 14–21. https://doi.org/10.1016/j.bios.2018.01.013

Tamir, A., Gangadharan, A., Balwani, S., Tanaka, T., Patel, U., Hassan, A., Benke, S., Agas, A., D'Agostino, J., Shin, D., Yoon, S., Goy, A., Pecora, A., & Suh, K. S. (2016). The serine protease prostasin (PRSS8) is a potential biomarker for early detection of ovarian cancer. *Journal of Ovarian Research, 9*(1), 1–13. https://doi.org/10.1186/s13048-016-0228-9

Tian, Z., Yang, C., Wang, W., & Yuan, Z. (2014). Shieldable tumor targeting based on pH responsive self-assembly/disassembly of gold nanoparticles. *ACS Applied Materials & Interfaces, 6*(20), 17865–17876. https://doi.org/10.1021/am5045339

Tripathi, P. P., Arami, H., Banga, I., Gupta, J., & Gandhi, S. (2018). Cell penetrating peptides in preclinical and clinical cancer diagnosis and therapy. *Oncotarget, 9*(98), 37252–37267. https://doi.org/10.18632/oncotarget.26442

Wallace, A. C., Laskowski, R. A., & Thornton, J. M. (1995). Ligplot: A program to generate schematic diagrams of protein-ligand interactions. *Protein Engineering, Design & Selection, 8*(2), 127–134. https://doi.org/10.1093/protein/8.2.127

Waltz, D. A., & Chapman, H. A. (1994). Reversible cellular adhesion to vitronectin linked to urokinase receptor occupancy. *The Journal of Biological Chemistry, 269*(20), 14746–14750. https://doi.org/10.1016/S0021-9258(17)36688-7

Wang, M., Löwik, D. W. P. M., Miller, A. D., & Thanou, M. (2009). Targeting the urokinase plasminogen activator receptor with synthetic self-assembly nanoparticles. *Bioconjugate Chemistry, 20*(1), 32–40. https://doi.org/10.1021/bc8001908

Wang, S., Liu, M., Zeng, D., Qiu, W., Ma, P., Yu, Y., Chang, H., & Sun, Z. W. (2014). Increasing stability of antibody via antibody engineering: Stability engineering on an anti-hVEGF. *Proteins: Structure, Function, and Bioinformatics, 82*(10), 2620–2630. https://doi.org/10.1002/prot.24626

Yan, Q., Zheng, H. N., Jiang, C., Li, K., & Xiao, S. J. (2015). EDC/NHS activation mechanism of polymethacrylic acid: Anhydride versus NHS-ester. *RSC Advances, 5* (86), 69939–69947. https://doi.org/10.1039/C5RA13844B

Zhao, B., Gandhi, S., Yuan, C., Luo, Z., Li, R., Gårdsvoll, H., de Lorenzi, V., Sidenius, N., Huang, M., & Ploug, M. (2015b). Mapping the topographic epitope landscape on the urokinase plasminogen activator receptor (uPAR) by surface plasmon resonance and X-ray crystallography. *Data in Brief, 5*, 107–113. https://doi.org/10.1016/j.dib.2015.08.027

Zhao, Gandhi, S., Yuan, C., Luo, Z., Li, R., Gårdsvoll, H., … Ploug, M. (2015a). Stabilizing a flexible interdomain hinge region harboring the SMB binding site drives uPAR into its closed conformation. *Journal of Molecular Biology, 427*(6), 1389–1403. https://doi.org/10.1016/j.jmb.2015.01.022